Magnetic Resonance Materials in Physics, Biology and Medicine
https://doi.org/10.1007/s10334-021-00937-w

RESEARCH ARTICLE

Comparative analysis of SINC-shaped and SLR pulses performance for contiguous multi-slice fast spin-echo imaging using metamaterial-based MRI

Ekaterina A. Brui[1] · Stanislas Rapacchi[2] · David Bendahan[2] · Anna E. Andreychenko[1,3]

Received: 12 February 2021 / Revised: 8 June 2021 / Accepted: 21 June 2021

Abstract

Objective To comparatively assess the performance of highly selective pulses computed with the SLR algorithm in fast-spin echo (FSE) within the current radiofrequency safety limits using a metamaterial-based coil for wrist magnetic resonance imaging.

Methods Apodized SINC pulses commonly used for clinical FSE sequences were considered as a reference. Selective SLR pulses with a time-bandwidth product of four were constructed in the MATPULSE program. Slice selection profiles in conventional T1-weighted and PD-weighted FSE wrist imaging pulse sequences were modeled using a Bloch equations simulator. Signal evolution was assessed in three samples with relaxation times equivalent to those in musculoskeletal tissues at 1.5T. Regular and SLR-based FSE pulse sequences were tested in a phantom experiment in a multi-slice mode with different gaps between slices and the direct saturation effect was investigated.

Results As compared to the regular FSEs with a conventional transmit coil, combining the utilization of the metadevice with SLR-based FSEs provided a 23 times lower energy deposition in a duty cycle. When the slice gap was decreased from 100 to 0%, the "slice cross-talk" effect reduced the signal intensity by 15.9–17.6% in the SLR-based and by 22.9–32.3% in the regular T1-weighted FSE; and by 0.0–6.4% in the SLR-based and by 0.3–9.3% in the regular PD-weighted FSE.

Discussion and conclusion SLR-based FSE together with the metadevice allowed to increase the slice selectivity while still being within the safe SAR limits. The "slice cross-talk" effects were conditioned by the number of echoes in the echo train, the repetition time, and T1 relaxation times. The approach was more beneficial for T1-weighted SLR-based FSE as compared to PD-weighted. The combination of the metadevice and SLR-based FSE offers a promising alternative for MR investigations that require scanning in a "Low-SAR" regime such as those for children, pregnant women, and patients with implanted devices.

Keywords Magnetic resonance imaging · Wrist · Radio waves

Introduction

Over the last few years, special attention has been paid to the use of metamaterial-based radiofrequency (RF) devices and metasurfaces (referred to as metadevices) in magnetic resonance imaging (MRI) [1–5]. This type of device is intended to dramatically improve the RF magnetic field transmission efficiency of the MR system. In addition, metadevices are expected to focus the RF magnetic field in an area of interest while shifting the electric field away from the patient's body. Accordingly, the RF energy deposition, a strictly regulated parameter in the MRI field, has been proved to be lower in comparison to conventional RF setups [4, 5]. One has to keep in mind that the level of specific absorption rate

✉ Ekaterina A. Brui
e.brui@metalab.ifmo.ru

[1] School of Physics and Engineering, ITMO University, Saint Petersburg, Russian Federation

[2] Centre de Résonance Magnétique Biologique et Médicale, Aix-Marseille Universite, CNRS, Marseille, France

[3] Department of Health Care of Moscow, Center of Diagnostics and Telemedicine Technologies, Research and Practical Clinical, Moscow, Russian Federation

Published online: 28 June 2021

(SAR) of electromagnetic energy depends not only on *how* the RF magnetic field is transmitted (i.e. what is the distribution of electric field provided by an RF coil) but also on the intensity of RF energy transmitted (i.e. *which* RF pulses and pulse sequences are employed during the image acquisition). That is why SAR becomes an issue at ultra-high field [6] considering that (i) body tissues absorb more RF energy at higher frequencies and (ii) the RF pulses power needed for a given magnetic field (B_1^+) level increases with respect to frequency. This issue may also be relevant in clinical fields when using pulse sequences containing high-amplitude pulses. As an example, adiabatic pulses, which are robust to radiofrequency inhomogeneities, have been used for an efficient fat suppression in musculoskeletal imaging at 3T [7] or for a robust saturation in first-pass cardiac perfusion MRI at 3T [8]. As a consequence, the SAR aspect usually limits the utilization of highly selective RF pulses [9] which deploy intense RF energy. Moreover, SAR regulations restrict the data acquisition speed and limit signal-to-noise ratio (SNR) by bounding the refocusing angle in fast pulse sequences, such as fast spin-echo (FSE) and single-shot fast spin-echo (SSFSE) [10, 11].

Even at a low magnetic field i.e. 1.5T, the SAR aspect can actually be a limit when one intends to use high amplitude and/or rapidly applying RF pulses. In that case, RF schemes used in the clinical settings have to be modified to fulfill the regulations [10, 12]. On that basis, any way of increasing the acceptable threshold of RF power and/or RF pulses frequency would be very attractive as long as the SAR is not modified. Metadevices open then up a very interesting opportunity to extend the limits of energy deposition of such pulse sequences, which could then be used in clinical MRI. Interestingly, a 48 times maximum local SAR reduction has been recently reported when a whole-body "birdcage" coil, which is the most commonly used transmit coil, was supplemented by a wireless metamaterial-based volumetric coil for hand and wrist MRI [4]. This substantial reduction could be used to improve the utilization of fast spin-echo (FSE) sequences which are the most SAR-demanding pulse sequences used in musculoskeletal clinical MRI. Efficient utilization of FSE sequences is most of the time restricted by the corresponding large SAR. In fact, FSE sequences combine spins excitation and rapid refocusing based on selective RF pulses with a certain narrow frequency band coupled to a local magnetic field gradient oriented perpendicularly to the desired slice (the slice selection gradient). A perfect rectangular slice profile is actually expected to make sure of the homogeneity of the localized excitation of spins. A non-rectangular excitation profile should lead to a decreased magnetization vector flip at the slice edges. In a multi-slice mode, the repeated refocusing may lead to an undesired direct saturation ("slice cross-talk") effect [9] when the spacing between the slices is not large enough. In multiple spin echo-based MR sequences, this type of bias is combined with a magnetization transfer effect, which can eventually lead to a large signal loss [13].

Dedicated highly selective pulses with a more rectangular excitation profile should reduce the error caused by poor slice selectivity but are associated with extensive energy deposition. The most widely used selective RF pulses in clinical MRI are truncated SINC-shaped pulses, apodized with Hamming or Hanning window [9]. The time-bandwidth product (TBW) of a SINC pulse defines the excited slice profile. A sufficiently rectangular profile can be reached at TBW > =6 [14]. However, this is only possible for long pulse duration and/or a large excitation bandwidth, which are both limited by multiple factors. First, the frequency bandwidth of a pulse is limited by the technical characteristics of the gradient system of a scanner (e.g. linear 22 mT/m—for 1.5T Magnetom Avanto in routine and 40 mT/m in research mode). Second, stretching RF pulses in time is deleterious to imaging as it causes signal loss and delays echo formation, eventually affecting image contrast. The most prevalent limitation is the limited energy deposition. Indeed, the increased TBW of a pulse is associated with a larger amplitude, which results in an increased SAR, a time-averaged measure proportional to the integral of the squared RF pulse waveform over the pulse duration [9]:

$$\mathrm{SAR} \sim \int_0^{Trf} B_1^2 * S^2(t)dt, \tag{1}$$

where B_1—is the pulse amplitude, T_{rf}—its duration, and $S(t)$—its waveform normalized to 1. For all these reasons, SINC-shaped pulses with high TBW are not commonly used in clinical MRI. The same situation occurs for other highly selective pulses with advanced waveforms such as those computed with the Shinnar–Le Roux (SLR) algorithm [15]. The SLR algorithm allows to design highly selective RF pulses with limited duration and strong constraints on the slice profile while leveraging digital filter design from the highly flexible polynomial formulation.

The aim of the present study was to comparatively assess the performance of these attractive highly selective pulses within the current RF safety limits thanks to the use of a metadevice. Fast spin-echo pulse sequences with clinical parameters and integrating selective RF pulses computed using the SLR algorithm were numerically simulated and implemented experimentally for phantom scanning using the metadevice previously used at 1.5T for wrist MRI [4].

Methods

Modeling

A Bloch equations simulator [16] was used as a basis for modeling the magnetization evolution in Matlab (The MathWorks, Natick, 2016). Using rotation and propagation matrices, the Bloch equations simulator iteratively calculates the magnetization vector components at each time point and for given instantaneous values of gradients and RF magnetic field amplitudes [17].

RF pulses

Regular apodized SINC pulses commonly used in clinical FSE sequences in low SAR mode on Siemens Magnetom Avanto MRI scanner were used as a reference. The parameters of RF and gradient pulses were extracted from the Siemens Magnetom Avanto MRI operating system and were used for the simulations. Excitation and refocusing profiles of these regular pulses were simulated. As a first step, the refocusing pulse profile computation was carried out for an ideal 90°-flip magnetization vector for the entire range of spatial positions [i.e. when longitudinal component $M_z(0) = 0$ and transverse component $M_{xy}(0) = 1$]. The rationale of this choice was to avoid the influence of a non-ideal excitation profile. The relaxation was also neglected during this phase.

The SLR pulses were constructed in the MATPULSE program [18]. The durations of the SLR pulses were identical to those of the reference pulses to keep the echo times unchanged. The excitation pulse was redesigned to provide no side lobes in the excitation profile by optimizing the ripples percentage in the pass and rejection bands. Its frequency bandwidth was similar to the one used for a regular excitation pulse. To increase the time-bandwidth product, and thus to increase the selectivity of the refocusing pulse, the frequency bandwidth of the 180° SLR pulse was chosen larger in comparison to the regular pulse. The limitation on the gradient amplitudes (2.2 G/cm) was taken into consideration while choosing the TBW of the pulse. We did not consider the maximal possible TBW (≈ 11) in order to leave the possibility of decreasing the slice thickness from 3 to 1 mm without exceeding the gradient limitations. Thus, the SLR pulse with TBW ≈ 4 was considered. The ripples percentages were chosen to obtain the sharpest refocusing profile without visible ripples in the passband.

FSE pulse sequence modeling

The signal evolution throughout the fast spin-echo sequence was modeled with the Bloch equations simulator for the slice selection only. We did not include the spatial signal encoding within the slice. The corresponding solutions were considered for a steady-state mode. At this stage, the excitation profile and the relaxation were taken into account.

Two FSE pulse sequences were computed as recommended for 1.5T wrist imaging by Siemens (https://www.siemens-healthineers.com). The parameters of the pulse sequence were as follows: repetition time TR = 550/3800 ms, echo time TE = 13/39 ms, excitation angle $\alpha = 90°$, refocusing angle $\beta = 180°$, echo spacing ES = 13 ms, echo train length ETL = 4/8. For a 2D version of the FSE sequence, each echo in the echo train conventionally acquires a new line in the k-space [19]. That is why, in FSE sequences, TE is the time of echo occurrence, which applies for the central part of the *k*-space and conditions signal contrast in the final image. For the T1-w/PD-w sequences we computed, it refers to the first and third echo, respectively.

Signal evolution was assessed for three samples (corresponded to 3 calibrated phantoms, Eurospin II, Diagnostic Sonar LTD, Scotland) with T1 and T2 relaxation times ranging from 329 to 992 ms and from 108 to 128 ms, respectively (see Table 1 for details). T1 times were chosen to represent three key compartments of MSK tissues: fat/bone marrow, cartilage, and muscle at 1.5T [20]. The other parameters were as follows: frequency offsets from − 50 to 50 Hz with a 1 Hz step; spatial positions of the magnetization vectors from − 15 to 15 mm with a 0.1 mm step (this set the dimensions of the sample and the number of points in it).

Slice profiles in FSE

The spatial profile of the transverse magnetization component M_{xy}, averaged over the entire range of frequency offsets, was considered as a signal profile in the direction of the slice selection (the slice profile). The slice profiles were calculated for regular and computed SLR pulses for each echo. In a real MRI experiment, the signal is acquired from the entire refocused area and not only from the width of the slice profile half-maximum. Therefore, it was necessary to

Table 1 Relaxation time of the samples

Phantom #	T1 (ms)	T2 (ms)	T1 of corresponding tissues (ms) [20]
P1	329	111	310/290 (fat/bone marrow)
P2	827	108	770 (cartilage)
P3	992	128	980 (muscle)

control the width of the entire refocused area (TH_1) and the signal refocused within this width (S_1—total signal) during the modeling and so to estimate how RF pulse shape affects the final images signal intensity. In the present work, the full width of the main lobe together with the first side lobes of the slice profile were considered as TH_1. At the same time, the sharpness of the slice profile was estimated through the ratio between the signal (S) accumulated within the desired slice thickness (TH) and the total signal S_1. The larger the ratio, the sharper the slice profile (for an ideal rectangular slice profile, this ratio would approach 1).

Experiments

The calculated SLR pulses were implemented in the software of the Siemens Magnetom Avanto MRI scanner. Pulse sequences with parameters similar to those used in the modeling were tested in 'Low SAR' mode for two cases i.e. with the regular pulses and with the engineered SLR pulses. The receiver gain was kept the same for all experiments, providing a possibility to compare absolute signal intensities. SAR automatically measured by the scanner was recorded.

The calibrated cylindrical gel phantoms (Eurospin II, length—11 cm, radius—3 cm), having the same relaxation times as in modeling (Table 1), were placed in a 3D-printed holder and positioned in the center of a metadevice as previously reported [4] (Fig. 1). Images were obtained in a multi-slice mode with seven slices (thickness—3 mm). In order to assess experimentally the effect of direct saturation that had not been modeled, different gaps between slices i.e. 100%, 50%, 25%, 10%, and 0% ("contiguous" slices) were considered. Slices were excited in one concatenation (in an interleaved order, predefined by the vendor). The average signal intensity was measured in a region of interest located in the medial (4th) slice of each multi-slice set and for each phantom. The results of the signal intensity measurements in the images with a 100% slice gap i.e. with a minimal direct saturation effect were compared with the modeling results.

To check the actual slice profiles in a single slice regime, an ACR [21] phantom was utilized. Profiles of the first echo in T1-w FSE and of the third echo in PD-weighted FSE were measured. Relaxation parameters of the phantom were unknown. A 10 mm-thick single slice was acquired perpendicular to the dedicated wedges height of the phantom. For each wedge, ascending and descending, an average intensity profile was extracted. This intensity profile was then spatially derived to compute the slice profiles. The ascending and descending profiles were eventually averaged in order to compensate for any remaining misalignment between the slice and the phantom. Since the ACR phantom boasts two sets of identical and coplanar wedges, these two measurements were averaged as well.

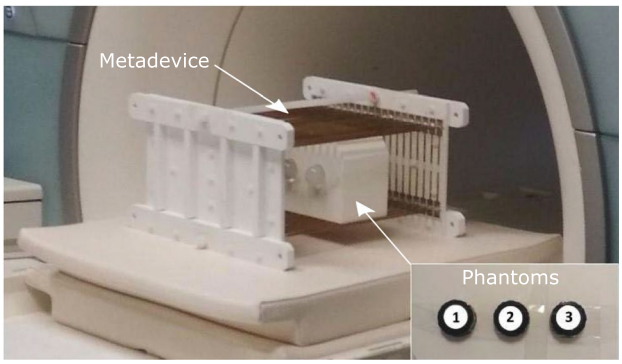

Fig. 1 Experimental setup for phantom measurements. The inset in the right bottom corner shows the order of phantom positioning in the holder

Results

Modeling

RF pulses

The RF and gradient pulses parameters used for the modeling of 3-mm wide slice selection in a regular FSE are summarized in Table 2. The obtained excitation and refocusing profiles for the regular pulses are depicted in Fig. 2a. Usually, the full-width at half-maximum of an excited profile is considered as the slice thickness (TH) [22]. However, for the particular case of FSE sequence, a lower than required gradient amplitude is commonly used

Table 2 Parameters of RF pulses used in modeling and experiment

Pulse type	Flip angle (°)	Length (ms)	BW (kHz)	Pass band ripples (%)	Rejection band ripples (%)	Pulse amplitude (μT)	G^a (mT/m)
Regular	90	2.816	1.36	–	–	7.93	7.3
Regular	180	3.840	0.68	–	–	13.68	5.3
SLR	90	2.816	1.36	1	1	8.33	7.3
SLR	180	3.840	1.06	0.5	0.5	23.99	8.2

[a]G is the amplitude of the slice-selective gradient necessary for refocusing a 3-mm width slice

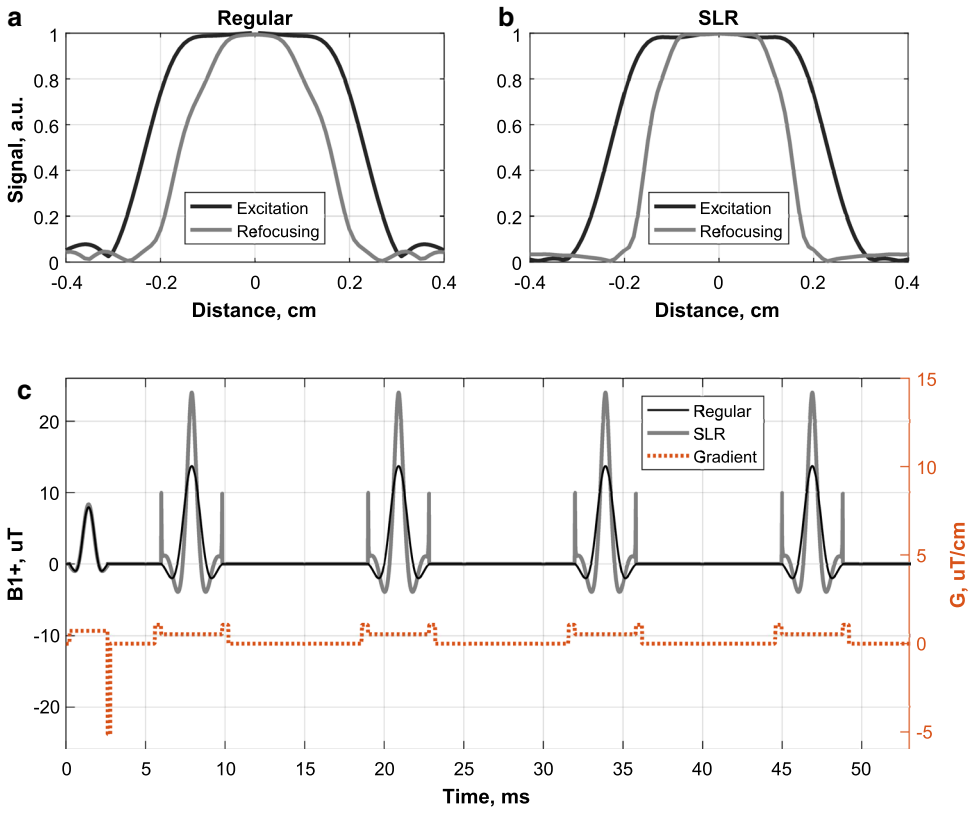

Fig. 2 Excitation (black curves) and refocusing (gray curves) profiles of regular pulses **a**, which are used by default in 1.5T Siemens Magnetom Avanto scanner for FSE in 'Low SAR' mode, and of the constructed SLR pulses **b** for a sample with neglected relaxation. **c** The evolution in time of RF amplitudes (black and gray curves for regular and SLR-based FSE, respectively) and slice selection, rewind, and crusher gradients (orange curve) that were generated. After the last pulse in the train, and until the end of the pulse sequence cycle, the arrays had zero value, except an additional crusher gradient at the end of the cycle (not shown), which was assumed to fully spoil the transverse magnetization

during the excitation in order to avoid a 3rd arm artifact caused by poor gradient linearity [23]. In that context, the slice thickness corresponds to a homogenously excited area of the profile (plateau) with less than 1% standard deviation of signal intensity.

The pulse profiles modeling showed that for the 90° SLR pulse, the optimal percentages of ripples in the pass-band and in the rejection band were both equal to 1%. Any further increase led to undesired ripples in the slice profile. Right after the excitation, the excited profile (Fig. 2b, black curve) was almost identical to a profile excited by a 90° regular pulse (Fig. 2a, black curve). Of interest, the side lobes typically observed for SINC pulses and large flip angles were not observed using SLR pulses. The energy produced by this SLR pulse was 5% higher than for the reference 90° pulse.

The frequency bandwidth of the refocusing SLR pulse was extended by a factor of 1.55 as compared to the regular pulse thereby allowing the time-bandwidth product to be increased to 4.06. The most suitable values of ripples percentage for the 180° pulse turned out to be 0.5%. The SLR pulse refocusing profiles are represented in Fig. 2b (gray curve). The corresponding calculated energy deposition was 73% higher than for the reference 180° SINC pulse. SLR pulses parameters are also listed in Table 2. Thanks to the bandwidth of the proposed refocusing SLR pulse together with the gradient amplitude limitations (max 22 mT/m), slice thickness could be decreased from 3.0 to 1.1 mm.

Slice profiles in FSE

Figure 2c illustrates the time-dependent changes of RF magnetic field amplitudes (black and gray curves for regular and SLR-based FSE, respectively) together with the slice selection, rewind, and crusher gradients (orange curve) that were generated in the T1-w FSE pulse sequence. Afterward and until the end of the pulse sequence cycle, the arrays had zero value, except an additional crusher gradient at the end of the cycle (not shown in Fig. 2c), which was assumed to fully spoil the transverse magnetization. A diagram for the PD-weighted FSE differed from Fig. 2c only by the number of refocusing and corresponding gradient pulses.

Slice profiles were simulated for three samples with different relaxation times (Table 1). Examples of the slice profiles (for sample P1) are displayed in Fig. 3 for the T1-weighted FSE integrating SINC (Fig. 3a) or SLR pulses (Fig. 3b) and for the PD-weighted FSE with SINC (Fig. 3c) or SLR pulses (Fig. 3d). For the first echo, the entire refocused area was wider for SINC (0.66 cm) as compared to SLR pulses (0.52 cm) and so for the whole set of samples. The corresponding total signal ratios (S_1^{SLR}/S_1^{REG}) for the first echo in T1-w FSE and for the third echo in PD-w FSE are summarized in Table 3. As indicated, signals were higher for the conventional FSEs as compared to the SLR-based sequences. Of interest, one could observe that this gain originated

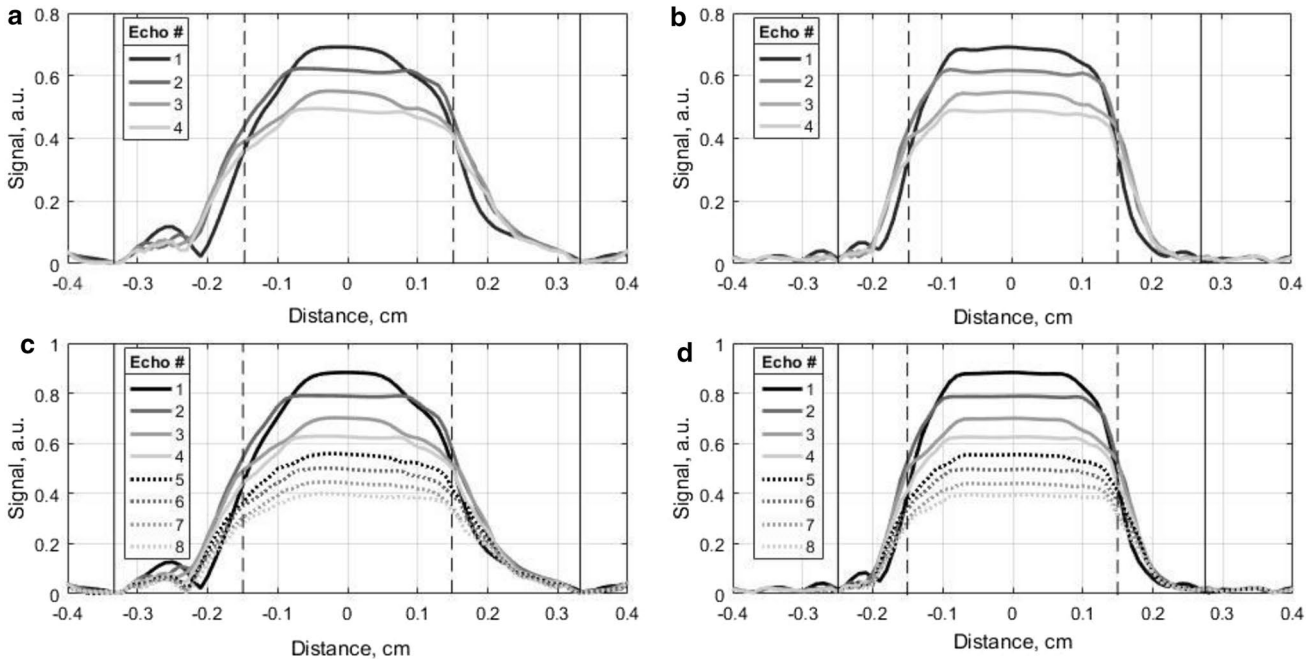

Fig. 3 Slice profiles of echo signals obtained for a sample with T1 = 329 ms in T1-weighted FSE modeling with regular pulses **a** and SLR pulses **b**, and in PD-weighted FSE modeling with regular pulses **c** and SLR pulses **d**. Black dashed vertical lines indicate the desired slice thickness (TH), black solid vertical lines indicate the entire refocused area of profiles (TH_1)

Table 3 Modeling results

Phantom	T1-weighted FSE, echo # 1	PD-weighted FSE, echo # 3
P1	0.98	0.94
P2	0.96	0.94
P3	0.96	0.94

The ratio of total signals (S_1^{SLR}/S_1^{REG}) obtained in modeling of SLR-based and regular variants of FSE for the echo signals forming the central part of *k*-space in each of the pulse sequences. Ratios are calculated for three samples, having different T1 times (P1—329 ms, P2—827 ms, and P3—992 ms)

from the refocusing of side lobes, i.e., from areas outside the desired slice. However, these asymmetric side lobes most probably resulted from computational errors. In the T1-w sequence, the S_1^{SLR}/S_1^{REG} ratio was slightly lower for higher T_1 relaxation times as a result of a larger saturation effects due to a relatively short TR. Also, the wider slice profile area was subjected to a larger refocusing angle (closer to 180°) when using SLR pulses.

As indicated in Fig. 4, the sharpness of the slice profiles was higher for all samples in SLR-based sequences. The sharpness was quite robust with respect to T1 changes in PD-w FSE, whereas for the T1-w sequence, it decreased with increasing T1 values.

Experiments

Phantom images were obtained using the metadevice and the pulse sequences with different slice gaps. Signal intensities measured in the phantoms are summarized in a diagram in Fig. 5. The standard deviation of the signal intensity measured in the ROIs did not exceed 2%. Using a 100% slice gap, the signal intensity obtained with the SLR-based pulse sequence was lower than for the regular sequence, and the measured S_1^{SLR}/S_1^{REG} ratios (Table 4) ranged from 0.87 to 0.99 in T1-w FSE, and from 0.86 to 0.92 in PD-w FSE for different phantoms. These ratios increased significantly for T1-w FSE when the slice gap was reduced to 0%: 0.98–1.04; and slightly for the PD-w FSE: 0.88–0.94.

For the T1-w FSE, when the slice gap was decreased from 100 to 0% the signal intensity dropped by 15.7–17.6% for different phantoms in the SLR-based sequence (Table 5). At the same time, the corresponding signal reduction was significantly worse for the regular pulse sequence 22.9–32.3%. For the PD-w FSE, the signal intensity drop was much lower—in the range of 0.03–6.4% (SLR) and 0.3–9.3% (Regular).

Using of SLR pulses increased the SAR recorded by the scanner by a factor of 2.1 for both T1-w and PD-w FSE sequences.

The measured slice profiles of the first echo in T1-w FSE and of the third echo in PD-w FSE are presented in Fig. 6. SLR pulses provided sharper slice selection and

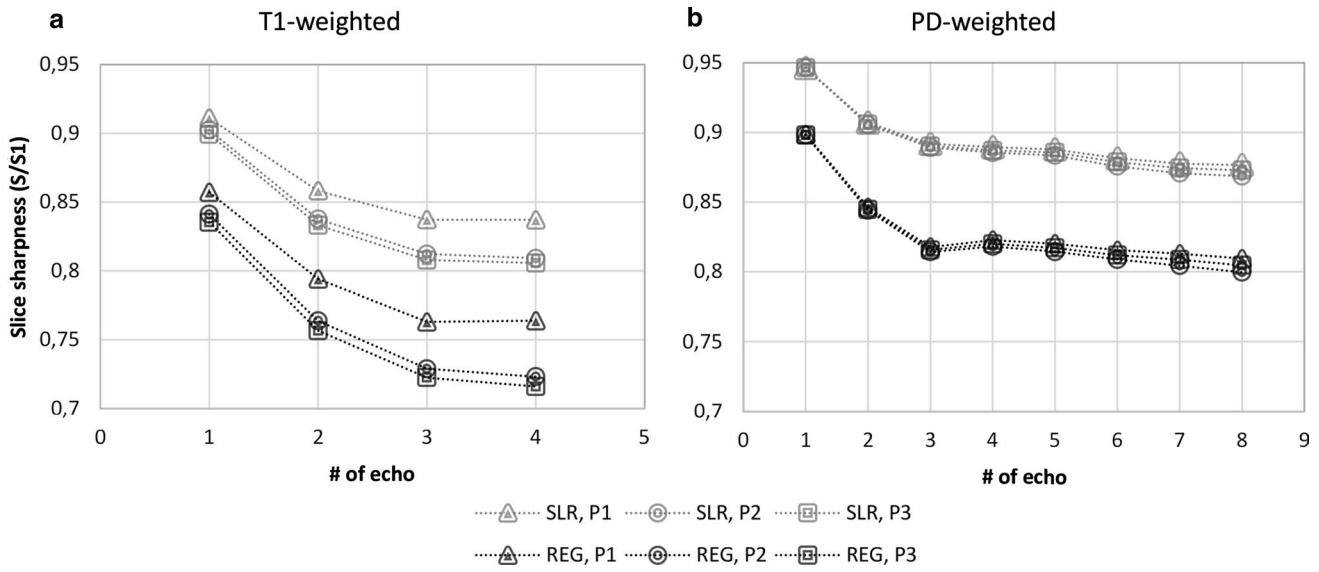

Fig. 4 Modeling results. The sharpness of slice profiles (S/S_1) calculated for T1-weighted **a** and PD-weighted **b** FSE in three samples with different T1 (P1—329 ms, P2—827 ms, and P3—992 ms). The gray curves correspond to the curves obtained for SLR-based sequences and the black ones—for the regular sequences

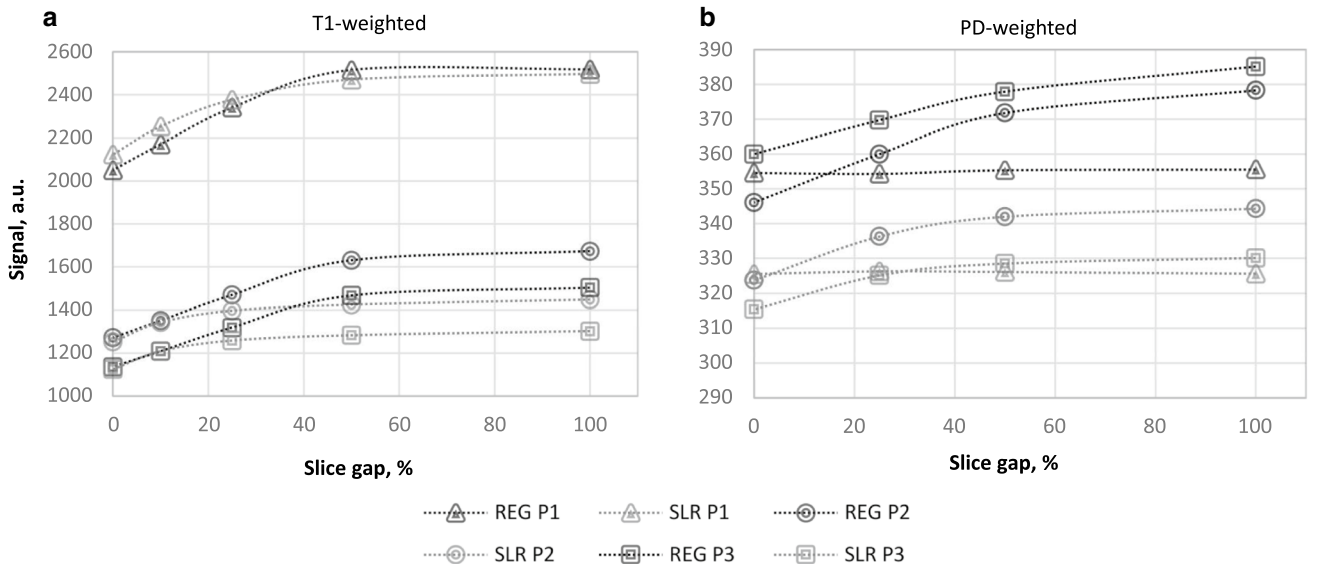

Fig. 5 Signal intensities measured in MR images obtained using regular FSE sequences (black markers) and SLR-based ones (gray markers) in a multi-slice scanning mode of T1-w FSE **a** and PD-w FSE **b** with different inter-slice gaps: 0%, 10%, 25%, 50%, 100%. The images were acquired with the same receiver gain that provided a possibility to compare absolute signal intensities. The dependences are presented for three phantoms with different T1 relaxation times: P1—329 ms (circle markers), P2—827 ms (squared markers), P3—992 ms (triangular markers). The absence of the direct saturation effect would correspond to no signal reduction when compare images acquired with 100% and 0% gaps

lower total signal for both echoes (Table 6). The sharpness difference was larger for the third echo in PD-w FSE as compared to the first echo in T1-w FSE and so as predicted by the modelization (see Figs. 3 and 4). However, the measured profiles did not fully reproduce the predicted ones with no side lobe for the regular case, and the values of the sharpness were higher than predicted. The ratios of total signals (S_1^{SLR}/S_1^{REG}) were in the predicted range (Table 6).

Table 4 Experimental results

Slice gap	100%		0%	
Phantom	T1-weighted FSE	PD-weighted FSE	T1-weighted FSE	PD-weighted FSE
P1	0.99	0.92	1.04	0.92
P2	0.87	0.86	0.98	0.88
P3	0.87	0.91	0.99	0.94

The ratio of total signals (S_1^{SLR}/S_1^{REG}) measured for SLR-based and regular variants of FSE pulse sequences in three phantoms, having different T1 times (P1—329 ms, P2—827 ms and P3—992 ms) when scanning with 100% and 0% slice gap

Table 5 Experimentally measured signal intensity drop (in %) due to the reduction of a slice gap from 100 to 0% of the slice thickness

Sequence	T1-weighted FSE		PD-weighted FSE	
Pulse type	Regular	SLR	Regular	SLR
P1	22.9	17.6	0.3	0.0
P2	31.6	15.7	7.0	4.7
P3	32.3	15.9	9.3	6.4
Mean	28.9	16.4	5.5	3.7
SD	5.3	1.1	4.7	3.3

Table 6 Experimentally measured parameters of the obtained for SLR-based and regular variants of FSE for the echo signals forming the central part of *k*-space in each of the pulse sequences: the sharpness of slice profiles (S/S_1) and the ratio of total signals (S_1^{SLR}/S_1^{REG})

Pulse sequence	T1-weighted FSE, echo # 1	PD-weighted FSE, echo # 3
S/S_1 (Regular)	0.89	0.87
S/S_1 (SLR)	0.93	0.94
S_1^{SLR}/S_1^{REG}	0.99	0.93

Slice profiles were measured in an ACR phantom

Discussion and conclusion

In the present study, we performed a comparative analysis in terms of RF energy deposition and slice selectivity for T1 and PD-weighted FSE sequences including either an SLR or a truncated SINC-based pulse. We eventually intended to use the corresponding sequences for musculoskeletal MRI using a metadevice, for which we previously reported a 2.4-fold SNR gain as compared to a conventional RF setup [4].

Let us consider the initial SAR generated in a duty cycle of a regular FSE with a conventional RF setup (when a full-body "birdcage" is used for transmission) as $\boldsymbol{SAR_1}$. We initially reported that using the metadevice the RF safety of a regular procedure was dramatically increased with a 48 times SAR reduction [4] i.e. $\boldsymbol{SAR_2 = SAR_1/48}$. Combining the metadevice with an FSE pulse sequence including SLR pulses provided a 2.1-fold increase regarding energy deposition considering the regular FSE as a reference ($\boldsymbol{SAR_2}$) i.e. $\boldsymbol{SAR_3 = SAR_2 * 2.1}$. On that basis, the latter setup still provided a 23 times lower energy deposition i.e. $\boldsymbol{SAR_3 = SAR_1/23}$ as compared to the conventional situation. Overall, the energy deposition related to the SLR-based pulse sequences performed with the metadevice was kept far below the initial RF safety limits.

Experimental results (Table 5) illustrated that the "slice cross-talk" effect was reduced in SLR-based FSEs in comparison to regular SINC-based FSEs. This was confirmative of the increased RF pulses selectivity shown by modeling (Fig. 3) and experiment (Fig. 6). This reduction was more prominent for the phantoms featuring cartilage and muscle due to long T1 relaxation times. This is in agreement with the findings of Constable et al. [13], who demonstrated that the direct saturation effect in multi-slice acquisition was more prominent in samples with higher T1/T2 ratios. Interestingly, the slice profiles obtained both from modeling and experiment demonstrated a reduction of the slice selectivity with an increasing number of echoes.

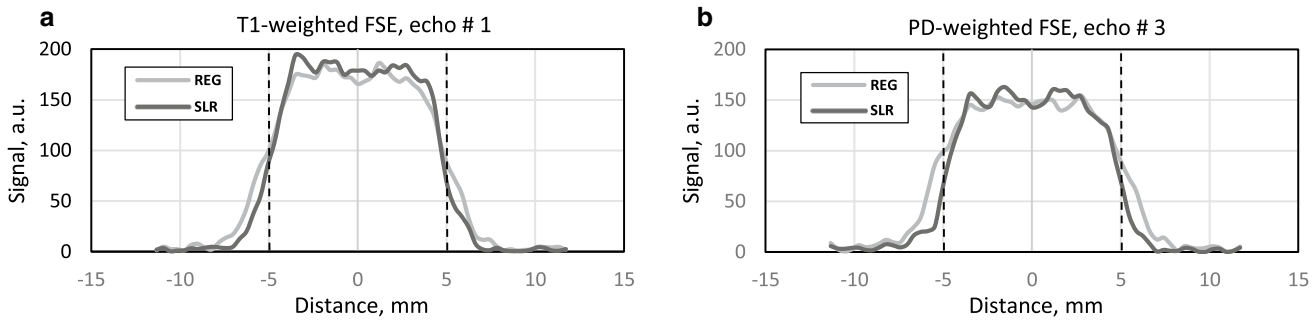

Fig. 6 Measured slice profiles of the first echo in T1-weighted FSE **a** and the third echo in PD-weighted FSE **b**. Black curves correspond to the pulse sequences with SLE RF pulses, and the gray ones—to the regular sequences with SINC pulses. Black dashed vertical lines indicate the slice thickness (10 mm) set by the operator

It was predicted from the modeling that the SLR-based FSE would provide a lower signal intensity than the regular one when the "slice cross-talk" effect was not taken into consideration. However, the experimentally measured (with 100% slice gap) signal intensity difference was higher than could be expected from the modeling for all cases. This difference most probably comes from the magnetization transfer (MT) effect, one of the main accounting factors of the signal loss in multi-slice acquisition (in both tissues and agarose-based solutions) even with significant slice gaps [13]. The widening of RF pulse bandwidth has been shown to amplify this effect [15]. Interestingly, using a PD-w TSE, including the largest number of refocusing pulses, this effect even led to a change in the image contrast (Fig. 5) and so when the regular refocusing pulses (bandwidth = 0.68 kHz) were replaced by SLR pulses (bandwidth = 1.06 kHz).

When considering a 0% slice gap (recommended for clinical applications) and using T1-w FSE, the signal intensity measured experimentally was similar for regular and SLR-based sequences (Table 4). In other words, the sharper profile of the SLR pulse allowed to acquire a higher signal intensity within the desired slice whereas the signal contribution from outside areas was lower (Figs. 3 and 6). Using PD-w FSE incorporating SLR pulses, this partial elimination of the "slice cross-talk" effect did not outperform the signal loss likely caused by MT effects. In that particular case, the corresponding sequence could not be considered beneficial. However, it should be taken into account that for in vivo applications, the MT rate in tissues differs from the one in agarose phantom. Thus, the relative impact of these two processes may be different from what is reported here and should be assessed.

The increased robustness of the slice selection provided by the combination of the metadevice and the SLR-based FSE is promising for clinical applications for which the SNR should be optimal. This is the case, for instance, for wrist imaging in rheumatoid arthritis (RA) and more specifically the assessment of cartilage loss [24, 25]. The cartilage loss criterion extracted from 3T MR images has been recently added to the rheumatoid arthritis MRI scoring system (RAMRIS). Of interest, images acquired at lower fields (1T and 1.5T) with conventional RF coils were reported to provide a poor resolution at the cartilage/bone interface so that the corresponding images could not be used for clinical purposes [26]. At 1.5T, only dedicated receive multichannel coils allow to achieve the proper resolution [25]. However, these coils are not broadly available mainly because of an elevated cost. A 2.4-fold SNR increase has been reported at 1.5T when using the volumetric metadevice as compared to a conventional flexible 4-channel receive coil [4]. Of interest, this metadevice was wirelessly coupled to the body birdcage coil, a coil available in all modern scanners. Of high interest for clinical applications, the combination of highly selective SLR pulses with the metadevice should provide an increased image resolution [27] and a higher slice selection accuracy. One has to acknowledge a limitation related to the fact that the current metadevice design does not allow to utilize parallel imaging technique, which could be used to accelerate image acquisition with multichannel receive arrays coil for simultaneous multi-slice imaging [28].

The studied pulse sequences did not fully utilize the benefit of SAR reduction opened up by the metadevice utilization. As the magnetization transfer effects depend on the macromolecular environment, the effects of TBW increase for in vivo applications should be studied. However, this leaves a room for a further improvement of image quality with, as a matter of example, an increased number of slices. Apart from the slice selectivity improvement for 2D FSE sequences used in a low-SAR mode, the opportunity of safely increasing RF pulse amplitude with the metadevice might be used for a further shortening of pulse duration in fast scanning mode for different pulse sequences. However, the gradient amplitude limitations and MT effects should be taken into consideration given that the pulse shortening is expected to be linked to a broadening of its frequency profile. Furthermore, the slab selection in 3D pulse sequences might also be improved so that aliasing effects [29] should be reduced. This should also be related to a shortening of the scan time given that slice oversampling could also be reduced. Taking into account that low gradients are needed to select a thick 3D slab, the limitation for slab selection gradient amplitudes will not be as strict as for slice selection in 2D FSE. This should allow to further increase the TBW of a selective excitation pulse [30]. The proposed approach may be transferred to higher fields, for instance, for improving targeted breast MRI with a help of dielectric resonators, which substantially reduce peak SAR values [31].

The present study provided both simulation and experimental evidence of an increased slice selectivity in MR images recorded using SLR-based FSE sequences combined with a metadevice and so within the safe SAR limits. A pronounced benefit has been experimentally shown for T1-weighted FSE—a pulse sequence, which is important for cartilage imaging. The larger magnetization transfer effect in agarose-based phantoms for PD-weighted sequence precluded from this improvement. In addition, the calculated energy deposition was decreased by a factor of 23 as compared to what has been previously reported for wrist imaging using a conventional RF setup [4]. The combination of the metadevice and SLR-based FSE offers an interesting alternative for MR investigations, which require scanning in a low SAR regime such as those for children, pregnant women, and patients with implanted devices (cardiac pacemakers, auditory devices, etc.).

Acknowledgements This work was supported by the Ministry of Education and Science of the Russian Federation (075-15-2021-592). EAB acknowledges the support received under the Ostrogradsky Programme of the French Embassy in Russia.

Author contributions Study conception and design: AEA. Acquisition of data: SR, EAB. Analysis and interpretation of data: EAB, SR. Drafting of manuscript: EAB. Critical revision: DB, AEA.

Declarations

Conflict of interest The authors declare that they have no competing interests.

Ethical approval For this type of study, no ethical approval is required

References

1. Radu X, Dardenne X, Craeye C (2007) Experimental results and discussion of imaging with a wire medium for MRI imaging applications. In: IEEE Antennas and Propagation Society, AP-S International Symposium (Digest) 4396793:5499–5502
2. Motovilova E, Sandeep S, Hashimoto M, Huang SY (2019) Water-tunable highly sub-wavelength spiral resonator for magnetic field enhancement of MRI coils at 1.5 T. IEEE Access 7:90304–90315
3. Brui EA, Shchelokova AV, Zubkov M, Melchakova IV, Glybovskiy SB, Slobozhanyuk AP (2018) Adjustable subwavelength metasurface for magnetic resonance imaging. Phys Status Solidi A 215:1700788
4. Shchelokova AV, Dobrykh DA, Glybovski SB et al (2018) Volumetric wireless coil based on periodically coupled split-loop resonators for clinical wrist imaging. Magn Reson Med 80:1726–1737
5. Schmidt R, Slobozhanyuk A, Belov P, Webb A (2017) Flexible and compact hybrid metasurfaces for enhanced ultra high field in vivo magnetic resonance imaging. Sci Rep 7:1678
6. Ladd M, Bachert P, Meyerspeer M, Moser E, Nagel AM, Norris DG, Schmitter S, Speck O, Straub S, Zaiss M (2018) Pros and cons of ultra-high-field MRI/MRS for human application. Prog Nucl Magn Reson Spectrosc 109:1–50
7. Kim D, Oesingmann N, McGorty K (2009) Hybrid adiabatic-rectangular pulse train for effective saturation of magnetization within the whole heart at 3 T. Magn Reson Med 62:1368–1378
8. Del Grande F, Santini F, Herzka DA, Aro MR, Dean CW, Gold GE, Carrino JA (2014) Fat-suppression techniques for 3-T MR imaging of the musculoskeletal system. Radiographics 34(1):217–233
9. Bernstein MA, King KF, Zhou XJ (2004) Handbook of MRI pulse sequences. Academic Press, Chicago
10. Hennig J, Weigel M, Scheffler K (2003) Multiecho sequences with variable refocusing flip angles: optimization of signal behavior using smooth transitions between pseudo steady states (TRAPS). Magn Reson Med 49:527–535
11. Loening AM, Saranathan M, Ruangwattanapaisarn N, Litwiller DV, Shimakawa A, Vasanawala SS (2015) Increased speed and image quality in single-shot fast spin echo imaging via variable refocusing flip angles. J Magn Reson Imaging 42:1747–1758
12. Borthakur A, Wheaton A, Charagundla SR, Shapiro EM, Regatte RR, Akella SVS, Kneeland JB, Reddy R (2003) Three-dimensional T1ρ-weighted MRI at 1.5 Tesla. J Magn Reson Imaging 17:730–736
13. Constable RT, Anderson AW, Zhong J, Gore JC (1992) Factors influencing contrast in fast spin-echo MR imaging. Magn Reson Imaging 10(4):497–511
14. Gras V, Abbas Z, Shah NJ (2013) Spoiled FLASH MRI with slice selective excitation: signal equation with a correction term. Concepts Magn Reson 42:89–100
15. Raddi A, Klose U (1999) Optimized shinnar-le roux RF 180° pulses in fast spin-echo measurements. J Magn Reson Imaging 9:613–620
16. Bloch Equations Simulator, http://mrsrl.stanford.edu/brian/blochsim/
17. Hargreaves BA, Vasanawala SS, Pauly JM, Nishimura DG (2001) Characterization and reduction of the transient response in steady-state MR imaging. Magn Reson Med 46(1):149–158
18. Matson GB (1994) An integrated program for amplitude-modulated RF pulse generation and re-mapping with shaped gradients. Magn Reson Imaging 12(8):1205–1225
19. Hennig J, Nauerth A, Friedburg H (1986) RARE imaging: a fast imaging method for clinical MR. Magn Reson Med 3(6):823–833
20. Kato H, Kuroda M, Yoshimura K, Yoshida A, Hanamoto K, Kawasaki S, Shibuya K, Kanazawa S (2005) Composition of MRI phantom equivalent to human tissues. Med Phys 32(10):3199–3208
21. https://www.acraccreditation.org/-/media/ACRAccreditation/Documents/MRI/LargePhantomGuidance.pdf
22. Brown RW, Cheng YCN, Haacke EM, Thompson MR, Venkatesan R (2014) A closer look at radiofrequency pulses. In: Magnetic resonance imaging physical principles and sequence design, 2nd edn. Wiley, New York
23. Nitz WR, Balzer T, Grosu DS, Allkemper T (2010) Principles of Magnetic Resonance. In: Reimer P, Parizel PM, Meaney JFM, Stichnoth FA (eds) Clinical MR Imaging. Springer, Berlin, Heidelberg
24. McQueen F, Clarke A, McHaffie A et al (2010) Assessment of cartilage loss at the wrist in rheumatoid arthritis using a new MRI scoring system. Ann Rheum Dis 69:1971–1975
25. Glinatsi D, Lillegraven S, Haavardsholm EA, Eshed I, Conaghan PG, Peterfy C, Gandjbakhch F, Bird P, Bøyesen P, Døhn UM, Genant HK, Østergaard M (2015) Validation of the OMERACT magnetic resonance imaging joint space narrowing score for the wrist in a multireader longitudinal trial. J Rheumatol 42(12):2480–2485
26. Peterfy CG (2001) Magnetic resonance imaging in rheumatoid arthritis: current status and future directions. J Rheumatol 28(5):1134–1142
27. Brui E, Lepekhina A, Chegina D, Bukkieva T, Efimtcev A, Andreychenko A (2020) Benefits of a wireless metamaterial-based radiofrequency coil for clinical wrist MRI. In: AIP Conference Proceedings, 5th International Conference on Metamaterials and Nanophotonics, METANANO 2020 2300(1):020012
28. Barth M, Breuer F, Koopmans PJ, Norris DG, Poser BA (2016) Simultaneous multislice (SMS) imaging techniques. Magn Reson Med 75(1):63–81
29. Graves MJ, Mitchell DG (2013) Body MRI artifacts in clinical practice: a physicist's and radiologist's perspective. J Magn Reson Imaging 38(2):269–287
30. Engström M, Mårtensson M, Avventi E, Skare S (2015) On the signal-to-noise ratio efficiency and slab-banding artifacts in three-dimensional multislab diffusion-weighted echo-planar imaging. Magn Reson Med 73:718–725
31. Shchelokova A, Ivanov V, Mikhailovskaya A, Kretov E, Sushkov I, Serebryakova S, Nenasheva E, Melchakova I, Belov P, Slobozhanyuk A, Andreychenko A (2020) Ceramic resonators for targeted clinical magnetic resonance imaging of the breast. Nat Commun 11:3840